ACS APPLIED MATERIALS & INTERFACES

Research Article

www.acsami.org

In Situ KPFM Imaging of Local Photovoltaic Characteristics of Structured Organic Photovoltaic Devices

Satoshi Watanabe,*[,†] Yasumasa Fukuchi,[‡] Masako Fukasawa,[‡] Takafumi Sassa,[§] Atsushi Kimoto,[∥] Yusuke Tajima,[⊥] Masanobu Uchiyama,[§,#] Takashi Yamashita,[‡] Mutsuyoshi Matsumoto,[†] and Tetsuya Aoyama*[,‡,§,⊥]

[†]Department of Materials Science and Technology, Tokyo University of Science, 6-3-1 Niijuku, Katsushika-ku, Tokyo 125-8585, Japan

[‡]Department of Pure and Applied Chemistry, Tokyo University of Science, Yamazaki 2641, Noda, Chiba 278-8510, Japan

[§]RIKEN, Hirosawa 2-1, Wako, Saitama 351-0198, Japan

[∥]Department of Chemistry of Functional Molecules, Faculty of Science and Engineering, Konan University, 8-9-1 Okamoto, Higashinada-ku, Kobe, Hyogo 658-8501, Japan

[⊥]RIKEN Innovation Center, Hirosawa 2-1, Wako, Saitama 351-0198, Japan

[#]Graduate School of Pharmaceutical Sciences, The University of Tokyo, 7-3-1 Hongo, Bunkyoku, Tokyo 113-0033, Japan

Supporting Information

ABSTRACT: Here, we discuss the local photovoltaic characteristics of a structured bulk heterojunction, organic photovoltaic devices fabricated with a liquid carbazole, and a fullerene derivative based on analysis by scanning kelvin probe force microscopy (KPFM). Periodic photopolymerization induced by an interference pattern from two laser beams formed surface relief gratings (SRG) in the structured films. The surface potential distribution in the SRGs indicates the formation of donor and acceptor spatial distribution. Under illumination, the surface potential reversibly changed because of the generation of fullerene anions and hole transport from the films to substrates, which indicates that we successfully imaged the local photovoltaic characteristics of the structured photovoltaic devices. Using atomic force microscopy, we confirmed the formation of the SRG because of the material migration to the photopolymerized region of the films, which was induced by light exposure through photomasks. The structuring technique allows for the direct fabrication and the control of donor and acceptor spatial distribution in organic photonic and electronic devices with minimized material consumption. This in situ KPFM technique is indispensable to the fabrication of nanoscale electron donor and electron acceptor spatial distribution in the devices.

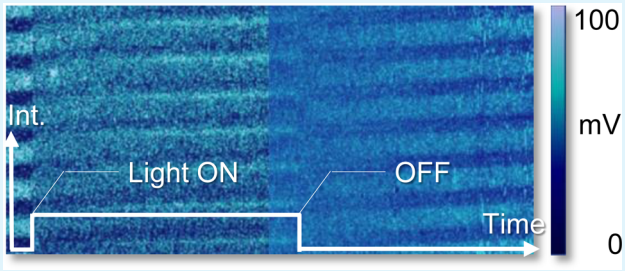

KEYWORDS: *organic photovoltaic device, kelvin probe force microscopy, surface relief grating, donor and acceptor spatial distribution, liquid carbazole*

INTRODUCTION

Bulk heterojunction photovoltaic devices have attracted much attention because of their tremendous potential for having a high-energy-conversion efficiency in organic thin-film photovoltaic devices.[1−13] Phase-separated structures of electron donors and electron acceptors (D/A) are formed in these devices, leading to an increase in the interfacial area between D/A compounds. Recently, D/A interface structures have been investigated using kelvin probe force microscopy (KPFM)[14−16] and conductive atomic force microscopy (AFM)[17−19] under illumination to understand the local photovoltaic characteristics of organic bulk heterojunction photovoltaic devices. From these results, the complicated and random distribution of donors and acceptors is considered to be a barrier that prevents smooth carrier transport to the electrode. To address this problem, ideally structured bulk heterojunction photovoltaic devices[20] have been fabricated for the control of the D/A spatial distribution using nanoimprinting,[21] microphase separation of diblock copolymers,[22,23] inorganic template nanostructures of TiO_x or ZnO_x,[24,25] surface relief grating (SRG) in active layers,[26] C_{60} nanocolumns,[27] Ag grating,[28] and a hole-blocking layer for conducting polymers.[29]

Following a report by Tripathy et al., SRGs have been widely utilized in organic materials to fabricate light-diffraction gratings, molds for imprinting, and refractive indices.[30] SRGs are formed in films that consist of an azobenzene polymer or monomer, which are mechanistically based on a photogradient effect.[31−33] Recently, SRGs have been formed in films that

Received: September 9, 2013
Accepted: January 22, 2014
Published: January 22, 2014

   dx.doi.org/10.1021/am4038992 | ACS Appl. Mater. Interfaces 2014, 6, 1481−1487

consist of other photochromic materials such as fluorine derivatives[34] and spiropyran,[35] and a few studies have already reported on the formation of SRGs in photopolymers.[36−38]

We previously reported the formation of photorefractive gratings in films made of the electron donor 3-formyl-9-vinylcarbazole (VCz(CHO)) and the electron acceptor 2,4,7-trinitro-9-fluorenone (TNF).[39] Periodic photopolymerization induced a gradient of carbazole density along the films, which resulted in the controlled formation of a periodic refractive-index pattern.[40] Additionally, VCz(CHO) films are very soft at room temperature, and these liquid carbazoles have recently been used as hole-transport materials,[41] organic light-emitting diodes,[42] and hybrid organic−inorganic bistable memory devices.[43] On the basis of these successes, we began investigating structured photovoltaic devices fabricated with VCz(CHO) and C_{61}-butyric acid methyl ester (PCBM) to take further advantage of the softness and photopolymerization properties of the liquid carbazole. We have demonstrated the formation of SRGs and D/A spatial distribution in the structured devices, which resulted in observably enhanced photocurrents.[39,44] D/A spatial distribution was formed in the structured photovoltaic devices, and PCBM molecules were highly distributed in the upper regions of the grating.[44−47]

Herein, we report on our investigation of the macroscopic and local photovoltaic properties in the structured photovoltaic devices. We also studied the morphology of the SRG to reveal the processes involved in SRG formation. The D/A spatial distribution, which serves as a smooth carrier pathway, brought about an enhancement in the photovoltaic characteristics of the structured devices. The SRGs and the D/A spatial distribution were obtained using simple periodic photopolymerization in the films. The local morphology and surface potential of the SRGs were analyzed by scanning AFM and in situ KPFM under illumination.

EXPERIMENTAL SECTION

Film Formation. VCz(CHO) and PCBM (MTR Limited) were used to fabricate the structured photovoltaic devices as p-type and n-type organic semiconductors, respectively (structures are depicted in Figure 1a). Indium tin oxide substrates were ultrasonicated sequentially in pure water, 2-propanol, acetone, and then chloroform for 10 min each; following that, they were kept in an ozone atmosphere for 3 min, which was generated by a UV/ozone cleaner, PL16-110D (SEN Lights Corp., Japan). VCz(CHO) and PCBM were dissolved in dichloromethane at a concentration of 20 mg mL^{-1} (80:20 wt %), and the solution was stirred for 2 h in the dark. Spin-coating was carried out at 1000 rpm for 10 s (Figure 1b).

Periodic Photopolymerization. Interference exposure was achieved using a continuous wave of a frequency-doubled Nd:YAG laser at 532 nm (Compass 315M-100, Coherent, Inc.) with an incident angle of 10° between the two laser beams for the periodic photopolymerization with an interference pattern at a period of about 3 μm. The VCz(CHO)/PCBM films used for the measurements of photocurrent action spectra and KPFM were periodically polymerized by an interference pattern of the two lasers with an intensity of 2 × 740 mW cm^{-2}, which resulted in the formation of an SRG at the respective diameters of 0.5 mm (Figure 1c, left). The film thickness was about 150 nm. To analyze the morphology in the photopolymerized and nonphotopolymerized regions of the films, the VCz(CHO)/PCBM films were exposed to single laser beams at 532 nm through photomasks with a small pattern (Figure 1c, right).

The films do not allow metal electrode deposition before subsequent photopolymerization procedures because the nonpolymerized region is soft. The structured films were cured with UV radiation using an ELC-410 light source (Electrolight, Ltd.) at 62 mW cm^{-2} in the 320−500 nm spectral range to polymerize the entire areas

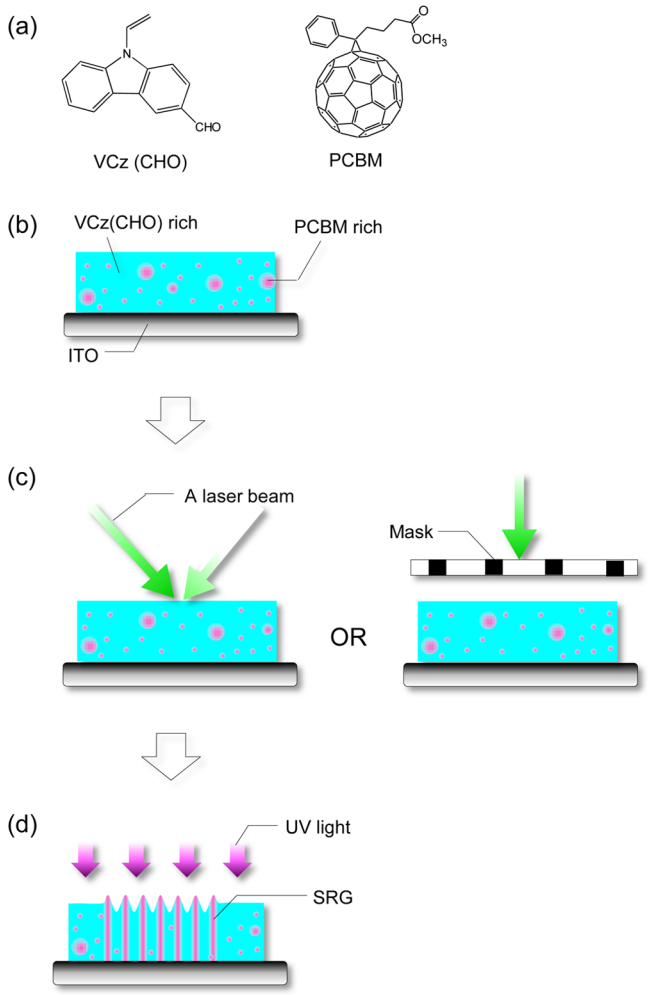

Figure 1. (a) Chemical structures of the photopolymerizable liquid carbazole of 3-formyl-9-vinylcarbazole (VCz(CHO)) and the fullerene derivative of C_{61}-butyric acid methyl ester (PCBM). (b−d) Schematic illustration of the fabrication of structured photovoltaic devices: (b) film-forming, (c) light exposure of the interference pattern from two laser beams at 532 nm or the laser beam through a photomask, and (d) polymerization using UV light over the entire area.

of the films. AFM and KPFM observations were performed after drying in a vacuum oven for 1 night (Figure 1d). A semitransparent Al electrode was deposited on the SRG and the homogeneous regions by vacuum deposition through shadow masks for the measurement of the photocurrent action spectra. For the selective deposition of the Al electrode on the SRGs, we performed periodic photopolymerization with an intensity of 2 × 175 mW cm^{-2} in wide areas, resulting in the formation of SRGs with a diameter of 3.3 mm.

Characterization. The photocurrent action spectra were measured with a Keithley Instruments model 6487. Intensity-controlled monochromatic light was obtained from a Xe lamp equipped with a monochromator (CT-10, Jasco, Inc.). The homogeneous films and structured films were irradiated with monochromatic light from the semitransparent Al electrode side for the photocurrent action spectra. A Dimension 3100 V (Digital Instruments) was used for AFM and KPFM observations of the structured films. Tapping mode AFM was carried out using a Pt/Ir-coated Si cantilever with a spring constant of 2.8 N m^{-1} and a resonance frequency of 75 kHz. For the KPFM observations, alternating current voltages were applied, mainly at 3 V, to the cantilever. We used the white light of a halogen lamp or band-pass-filtered monochromated light to measure the surface potential under light illumination.

RESULTS AND DISCUSSION

We previously reported the enhanced short-circuit photocurrents in structured photovoltaic devices with a 532 nm incident laser beam for the formation of the D/A spatial distribution.[44,45] Here, we investigate the photocurrent action spectra of structured BHJ devices.

The absorption bands for the UV−vis absorption spectra of VCz(CHO)/PCBM films (83:17 wt % and PCBM-free) ranged in the UV region (Figure 2a). The maximal absorption occurred at about 250 nm and can be attributed to VCz(CHO). Absorbance in the visible region was slightly increased by doping with PCBM. The diffraction efficiency of the SRGs is at most 1.5% according to our previous study,[44] suggesting that the effect of the grating structures is weak in the UV−vis absorption and indicating that the influence of diffraction to absorption is small and the effect of the increase in effective optical path length is limited (Figure S1). Figure 2b shows the photocurrent action spectra of the structured and as-prepared films of VCz(CHO)/PCBM (80:20 wt %) under light illumination. The photocurrent of the structured films is larger than that of the homogeneous films in the UV region. These results demonstrate that the structured photovoltaic devices provide enhanced photocurrents because of the D/A spatial distribution, as previously reported.[44,45]

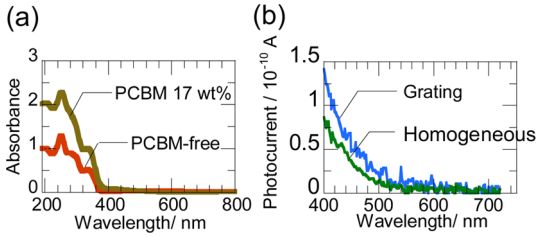

Figure 2. (a) UV−vis absorption spectra of VCz(CHO)/PCBM films (83:17 wt % and PCBM-free). (b) Photocurrent action spectra of the grating and homogeneous regions of VCz(CHO)/PCBM films (80:20 wt %) under monochromatic light illumination.

Here, we discuss how in situ KPFM provides insight into the local photovoltaic properties of the structured films under light illumination.

Figure 3 shows the AFM and KPFM images as well as the KPFM profile of the VCz(CHO)/PCBM film (80:20 wt %) grating both in the dark and under illumination. During the first 3 min, the observations were carried out in the dark. The KPFM image shows the periodic surface potential modulation that is based on the D/A spatial distribution in the films. The depth of the surface potential modulation ($V_d = V_u - V_l$, where V_u and V_l signify the surface potential of the upper and lower regions of the grating, respectively) is about 40 mV. After 3 min, the film was irradiated by a white-light source. The AFM image was not affected by light irradiation. However, KPFM images show the change in the surface potential distribution after illumination with white light. After 40 min, the surface potential of the upper region became smaller than that of the lower region, which resulted in a saturated V_d that reached approximately −20 mV. Charge generation occurs over the entire area of the film's, and the electrons migrate to the PCBM-rich regions, which results in the formation of PCBM anions.[43−45] However, the average surface potential (V_a) decreased from 140 to 100 mV. The observed negative shift of the average surface potential is due to the effect of holes drifting into the ITO electrode because of the films higher hole mobility than electron mobility, as previously reported.[14,15,49] Figure 3d shows a KPFM image of the grating after the white light was turned off, where the surface potential distribution gradually returned to the pre-illuminated state. This reversibility serves to indicate the charge generation under illumination and charge collection. The charging and discharging intervals are much longer than the photoinduced charge-generation intervals, indicating the occurrence of deep electron charge trapping and detrapping.[50,51] These phenomena can be seen both in the surface potential in the upper and lower regions of the gratings and the average surface potential, as shown in Figure 3e. These demonstrate that local photovoltaic characteristics can be observed in the structured devices.

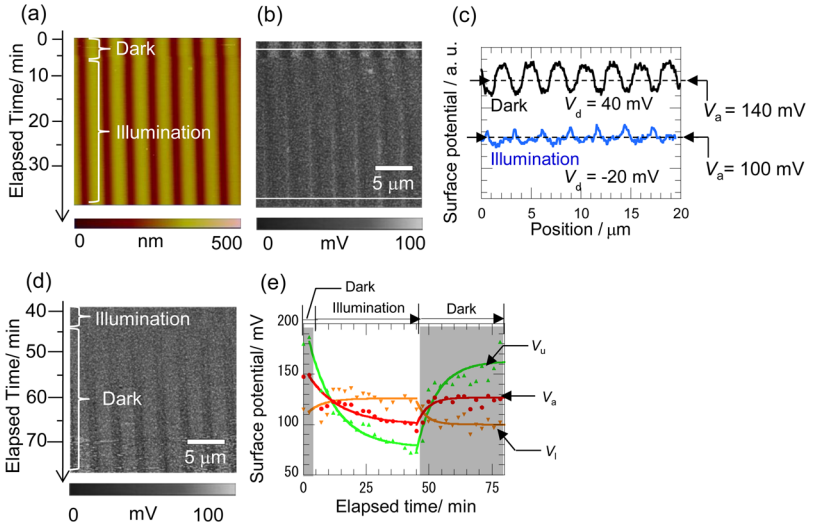

Figure 3. (a) AFM and (b) KPFM images and (c) their profiles for VCz(CHO)/PCBM film (80:20 wt %) in the dark and under illumination from a white-light source. The profiles were obtained from white lines in the (b) KPFM image. (d) KPFM image of the grating after the white light was turned off. (e) Time evolution of the surface potential in the upper and lower regions of the grating and the surface potential averaged in the imaging area. The charging and discharging processes are fitted with single exponential functions.

dx.doi.org/10.1021/am4038992 | ACS Appl. Mater. Interfaces 2014, 6, 1481−1487

To investigate the correlation between surface potential and wavelength of the incident light, we measured the surface potential of the grating under irradiation with monochromatic light of various wavelengths.

The plots of surface potential differences (ΔV_d and ΔV_a) versus light intensity at various wavelengths, as depicted in Figure 4a,b, use the differences in V_d or V_a between the

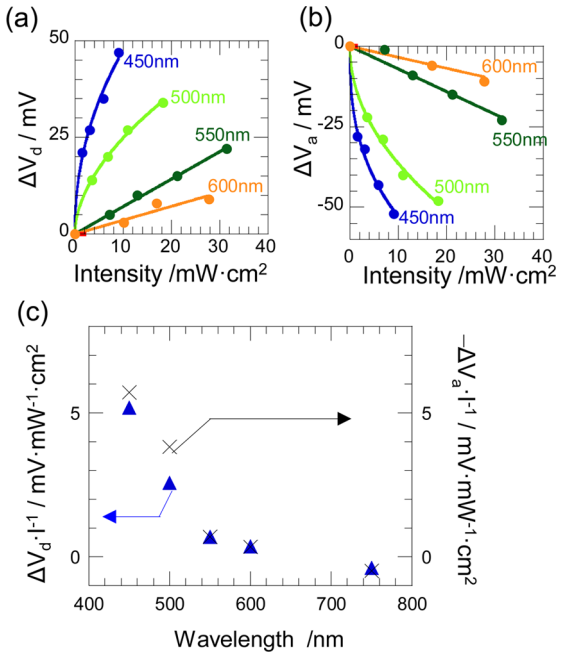

Figure 4. (a) Surface potential difference, ΔV_d, and (b) average surface potential difference, ΔV_a, plotted against the intensities of incident light and fitted with a sublinear function. (c) Surface potential action spectra of ΔV_d and ΔV_a normalized with respect to light intensity. The cantilever repeatedly scanned at the same position of the grating.

illuminated conditions and dark conditions. ΔV_d and ΔV_a were calculated by averaging each ΔV_d and ΔV_a value in the SRGs after saturating the surface potential under light illumination; the errors are too small to represent as error bars. The noticeable dependence of the surface potential on light intensity is consistent with the reported findings in a previous study on polyfluorene-based photodiodes.[48] Figure 4c shows the surface potential action spectra of ΔV_d and ΔV_a normalized to their light intensities. These surface potential action spectra are in good agreement with the absorption spectra and photocurrent action spectra shown in Figure 2, panels a and b, respectively. These results demonstrate that local photovoltaic characteristics are clearly observed in the structured photovoltaic devices.

We also closely investigated the morphology of the structured films fabricated by exposing them to an interference pattern of two laser beams.

Figure 5a shows an AFM image of the edge of the grating in the VCz(CHO)/PCBM films (80:20 wt %). The film was partly scratched to measure its thickness. The height between the upper and lower regions of the grating was about 100 nm. The average thickness of the SRG was 150 nm, which is almost coincident with that of the homogeneous regions. This suggests that periodic photopolymerization gives rise to the formation of the regions where the film thickness alternately increases and

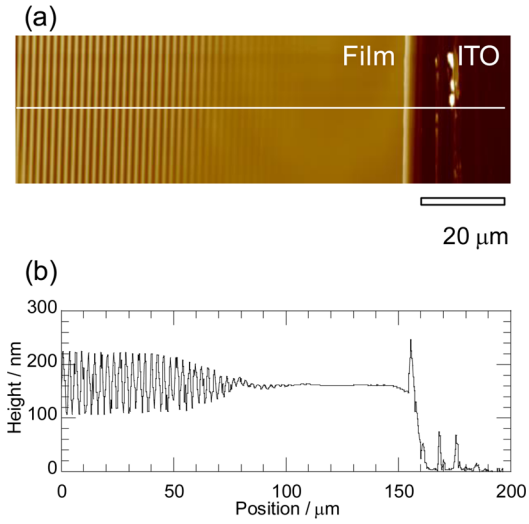

Figure 5. (a) AFM image and (b) cross-sectional view of the edge of the grating in a VCz(CHO)/PCBM film (80:20 wt %). The film was scratched with a knife for the height measurements between the films and the ITO substrates. The AFM observations were carried out with a VN-8000 microscope (KEYENCE).

decreases. These results indicate the occurrence of material migration from one region to another during the photopolymerization.

Alternatively, we investigated the morphology and surface potential of the VCz(CHO)/PCBM films fabricated by light illumination through a photomask to determine the direction of material migration.

Figure 6a shows an AFM image and the cross-sectional view of a VCz(CHO)/PCBM film irradiated with a laser beam through a photomask having an interdigitated pattern. The lower half of the image is of the section of the film completely covered by the photomask, which resulted in no occurrence of photopolymerization by the laser beam. The upper half of the image shows that the photopolymerized regions are higher than the nonphotopolymerized regions (covered with line masks) by about 50 nm, which resulted in increased heights for the photopolymerized regions of the films. Additionally, the average heights in the profile nearly coincide with the film thicknesses. A study reported by Veltri et al. may aid in understanding the formation mechanism of the grating in photopolymer films.[52] The distribution of materials in the photopolymerized films is associated with the material migration from the nonphotopolymerized region to the photopolymerized regions, which eventually leads to the formation of the gratings. Slow photopolymerization allows the concentration of the monomers to be spatially modulated. The diffusion of monomers is the main mechanism that determines the formation of the grating. We assume that the gratings consisting of carbazole are formed according to a similar mechanism. After the photochemical reaction with the vinyl group, monomeric carbazoles are converted to dimers or polymers in the films containing acceptors.[53,54] Photochemical reactions also lead to PCBM dimers or oligomers under UV or visible-light irradiation.[55,56] Several products appeared to be intricately formed, as indicated by high-performance liquid chromatography (HPLC) results (Figure S2). These results indicated that material migration from the nonphotopolymerized regions to the photopolymerized regions occurred during illumination.

dx.doi.org/10.1021/am4038992 | ACS Appl. Mater. Interfaces 2014, 6, 1481−1487

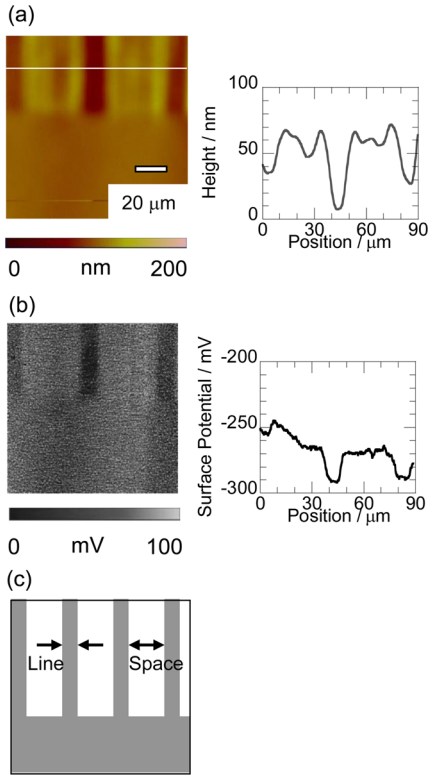

Figure 6. (a) AFM and (b) KPFM images and profile of the VCz(CHO)/PCBM film (80:20 wt %) photopolymerized by illumination at 532 nm through a photomask with a (c) pattern of line/space (8/32 μm).

Figure 6b shows a KPFM image and the profile of the same film. The surface potential of the photopolymerized regions is higher than that of the nonphotopolymerized regions covered with line masks by about 30 mV, which indicates that material migration during the polymerization affected the relative distribution of VCz(CHO) and PCBM. The surface potential increases linearly with the PCBM concentration.[45] Because the surface potential in the photopolymerized region is higher than that of the nonphotopolymerized region, the PCBM concentration in the upper region is supposed to be higher than in the lower region. Slow photopolymerization rates lead to the formation of SRG because of material migration from the nonphotopolymerized to the photopolymerized regions.[52] The rate of PCBM photopolymerization should be lower than that of VCz(CHO) in the films. These results demonstrated that material migration of the PCBM predominantly proceeded from the nonphotopolymerized regions to the photopolymerized regions.

Imaging the vertical distribution of D/A might be required because inhomogeneous structures are often formed in organic BHJ photovoltaic devices.[59] However, according to Luria et al., surface potential is considered to be the average work function of films in the vertical direction, and it's hard to discuss the vertical distribution. However, because a very small absorbance around 530 nm was observed in the VCz(CHO) and PCBM films shown in Figure 2a, photopolymerization was expected to be performed uniformly through the films, and D/A spatial distribution might not be formed in the vertical direction by periodic photopolymerization.

It should be noted that surface potential was affected by the morphology,[58] chemical species,[14−16,45] and dipole moments.[59] We investigated the dependence of surface potential on the photochemical reaction of the carbazole and PCBM, and the morphologies of the grating can be seen in Figures S3 and S4, respectively. The small morphological effect may be explained by considering that the ratio of the height to the period in the SRGs is smaller than that of the height to the curvature radius in the KPFM probes. The surface potential did not change in the films after irradiation using a single laser beam, which signifies that no material migration occurs. These results give no indication that the surface potential was influenced by photochemical reactions and morphological effects in our observations; this indicates that the surface potential can be related to the concentration of PCBM in the grating.

CONCLUSIONS

We have demonstrated the local photovoltaic characteristics of the D/A spatial distribution of our structured photovoltaic devices. The D/A spatial distribution was formed in the VCz(CHO)/PCBM films exposed to an interference pattern generated by two laser beams. The SRGs formed in the films because of material migration from the nonphotopolymerized region to the photopolymerized region. KPFM observations show the formation of the surface potential distribution in the SRGs of the films in the dark. Under illumination, surface potential, V_d, and the average surface potential, V_a, significantly change because of the generation of PCBM anions and charge drifting to the ITO electrode, respectively. The correlation between the surface potential and light wavelength almost coincide with the absorption and photocurrent action spectra. These results demonstrate that reversible local photovoltaic characteristics are observed in the SRGs of the structured photovoltaic devices.

This technique allows for the direct fabrication of D/A spatial distribution in the film, resulting in the formation of D/A spatial distribution with small material consumption and few fabrication steps when compared to conventional techniques. In addition, local photovoltaic properties can be imaged by KPFM observation under monochromatic light illumination, which enables the acquisition of photocurrent action spectra and, consequently, the photovoltaic characteristics in the local regions of the structured films. Furthermore, development of SRG structures will improve the device efficiency in organic photovoltaic devices and organic light-emitting diodes because of an increase in the D/A interfacial areas and optical path length. This technique is applicable to the investigation of local electrostatic properties in organic field-effect transistors, organic light-emitting diodes, and other types of organic photovoltaic devices; overall, this will contribute to nanofabrication and nanoscale observations in optoelectronics and photonic devices.

ASSOCIATED CONTENT

Supporting Information

Absorption spectra of the SRGs and the homogeneous region of the VCz(CHO)/PCBM films, HPLC chromatograms to investigate VCz(CHO) and PCBM before and after UV irradiation, KPFM measurement to study the surface potential change after irradiation with a 532 nm laser and UV light, and AFM observation for analysis of the morphological effect on the surface potential. This material is available free of charge via the Internet at http://pubs.acs.org.

AUTHOR INFORMATION

Corresponding Authors

*E-mail: watasato@rs.noda.tus.ac.jp (S.W.).
*E-mail: taoyama@riken.jp (T.A.).

Author Contributions

The manuscript was written through contributions of all authors. All authors have given approval to the final version of the manuscript.

Notes

The authors declare no competing financial interest.

ACKNOWLEDGMENTS

We are grateful to Dr. P. André from the University of St. Andrews and Prof. J. C. Ribierre from Kyushu University for careful and helpful discussions. The authors thank Keyence Corporation for the VN-8000 AFM microscope used to analyze SRGs.

ABBREVIATIONS

D/A, electron donors and electron acceptors
SRGs, surface relief gratings
VCz(CHO), 3-formyl-9-vinylcarbazole
TNF, 2,4,7-trinitro-9-fluorenone
PCBM, C_{61}-butyric acid methyl ester
AFM, atomic force microscopy
KPFM, kelvin probe force microscopy

REFERENCES

(1) Yu, G.; Gao, J.; Hummelen, J. C.; Wudl, F.; Heeger, A. J. *Science* **1995**, *270*, 1789−1791.
(2) Ma, W.; Yang, C.; Gong, X.; Lee, K.; Heeger, A. J. *Adv. Funct. Mater.* **2005**, *15*, 1617−1622.
(3) Li, G.; Shrotriya, V.; Hung, J.; Yao, Y.; Moriarty, T.; Emery, K.; Yang, Y. *Nat. Mater.* **2005**, *4*, 864−868.
(4) McNeill, C. R.; Greenham, N. C. *Adv. Mater.* **2009**, *21*, 3840−3850.
(5) Kim, Y.; Cook, S.; Tuladhar, S. M.; Choulis, S. A.; Nelson, J.; Durrant, J. R.; Bradley, D. D. C.; Giles, M.; Mcculloch, I.; Ha, C.; Ree, M. A. *Nat. Mater.* **2006**, *5*, 197−203.
(6) Peumans, P.; Uchida, S.; Forrest, S. R. *Nature* **2003**, *425*, 158−162.
(7) Yang, X.; Loos, J.; Veenstra, S. C.; Herhees, W. J. H.; Wienk, M. M.; Kroon, J. M.; Michels, M. A. J.; Janssen, R. A. J. *Nano Lett.* **2005**, *5*, 579−583.
(8) Hoppe, H.; Sariciftei, N. S. *J. Mater. Chem.* **2006**, *16*, 45−61.
(9) Hoppe, H.; Sariciftei, N. S. *J. Mater. Res.* **2004**, *19*, 1924−1945.
(10) Blom, P. W. M.; Mihailetchi, V. D.; Koster, L. J. A.; Markov, D. E. *Adv. Mater.* **2007**, *19*, 1551−1566.
(11) Rousseau, T.; Cravino, A.; Bura, T.; Ulrich, G.; Ziessel, R.; Roncali, J. *Chem. Commun.* **2009**, *45*, 1673−1675.
(12) Kronenberg, N. M.; Deppisch, M.; Würthner, F.; Lademann, H. W. A.; Deing, K.; Meerholz, K. *Chem. Commun.* **2008**, *44*, 6489−6491.
(13) Gomez, E. D.; Barteau, K. P.; Wang, H.; Toneyc, M. F.; Loo, Y. *Chem. Commun.* **2011**, *47*, 436−438.
(14) Hoppe, H.; Glatzel, T.; Niggemann, M.; Hinsch, A.; Lux-Steiner, M. C.; Sariciftci, N. S. *Nano Lett.* **2005**, *5*, 269−274.
(15) Liscio, A.; Luca, G. D.; Nolde, F.; Palermo, V.; Müllen, K.; Samori, P. *J. Am. Chem. Soc.* **2008**, *130*, 780−781.
(16) Spadafora, E. J.; Demadrille, R.; Ratier, B.; Grevin, B. *Nano Lett.* **2010**, *10*, 3337−3342.
(17) Coffey, D. C.; Reid, O. G.; Rodovsky, D. B.; Bartholomew, G. P.; Ginger, D. S. *Nano Lett.* **2007**, *7*, 738−744.
(18) Leever, B. J.; Durstock, M. F.; Irwin, M. D.; Hains, A. W.; Marks, T. J.; Pingree, L. S. C.; Hersam, M. C. *Appl. Phys. Lett.* **2008**, *92*, 013302-1−013302-3.
(19) Guide, M.; Dang, X. D.; Nguyen, T. Q. *Adv. Mater.* **2011**, *21*, 2313−2319.
(20) Günes, S.; Neugebauer, H.; Sariciftci, N. S. *Chem. Rev.* **2007**, *107*, 1324−1338.
(21) Kim, M. S.; Kim, J. S.; Cho, J. C.; Shtein, M.; Guo, L. J.; Kim, J. *Appl. Phys. Lett.* **2007**, *90*, 123113-1−123113-3.
(22) Jenekhe, S.; Chen, X. L. *Science* **1998**, *279*, 1903−1907.
(23) Hadziioannou, G.; von Huttern, F. *Semiconducting Polymers: Chemistry, Physics, and Engineering*; Wiley-VCH: Weinheim, Germany, 2000; Vol. *1*, pp 100−120.
(24) Coakley, K.; McGehee, M. D. *Appl. Phys. Lett.* **2003**, *83*, 3380−3382.
(25) Olsa, D. C.; Piris, J.; Collins, R. T.; Shaheen, S.; Ginley, D. *Thin Solid Films* **2006**, *496*, 26−29.
(26) Li, K.; Zhen, H.; Huang, Z.; Li, G.; Liu, X. *ACS Appl. Mater. Interfaces* **2012**, *4*, 4393−4397.
(27) Thomas, M.; Worfolk, B. J.; Rider, D. A.; Taschuk, M. T.; Buriak, J. M.; Brett, M. J. *ACS Appl. Mater. Interfaces* **2011**, *3*, 1887−1894.
(28) Baba, A.; Aoki, N.; Shinbo, K.; Kato, K.; Kaneko, F. *ACS Appl. Mater. Interfaces* **2011**, *3*, 2080−2084.
(29) Meier, R.; Birkenstock, C.; Palumbiny, C. M.; Müller-Buschbaum, P. *Phys. Chem. Chem. Phys.* **2012**, *14*, 15088−15098.
(30) Kim, D. Y.; Tripathy, S. K.; Li, L.; Kumar, J. *Appl. Phys. Lett.* **1995**, *66*, 1166−1168.
(31) Natansohn, A.; Rochon, P. *Chem. Rev.* **2002**, *102*, 4139−4175.
(32) Bian, S.; Williams, J. M.; Kim, D. Y.; Li, L.; Balasubramanian, S.; Kumar, J.; Tripathy, S. *J. Appl. Phys.* **1999**, *86*, 4498−4508.
(33) Viswanathan, N. K.; Kim, D. Y.; Bian, S.; Williams, J.; Liu, W.; Li, L.; Samuelson, L.; Kumarab, J.; Tripathy, S. K. *J. Mater. Chem.* **1999**, *9*, 1941−1955.
(34) Okano, K.; Ogino, S.; Kawamoto, M.; Yamashita, T. *Chem. Commun.* **2011**, *47*, 11891−11893.
(35) Ubukata, T.; Takahashi, K.; Yokoyama, Y. *J. Phys. Org. Chem.* **2007**, *20*, 981−984.
(36) Kang, S. W.; Sprunt, S.; Chien, L. C. *Chem. Mater.* **2006**, *18*, 4436−4441.
(37) Ubukata, T.; Yamaguchi, S.; Yokoyama, Y. *Chem. Lett.* **2007**, *36*, 1224−1225.
(38) Zhao, D.; Xu, Z.; Wang, G.; Cao, H.; Li, W.; He, W.; Huang, W.; Yang, Z.; Yang, H. *Phys. Chem. Chem. Phys.* **2010**, *12*, 1436−1439.
(39) Aoyama, T.; Fukuchi, Y.; Sassa, T.; Yamashita, T.; Wada, T. *J. Photopolym. Sci. Technol.* **2007**, *20*, 93−96.
(40) Sassa, T.; Aoyama, T.; Zhang, Y.; Wada, T.; Sasabe, H. *Proc. SPIE* **1998**, *3471*, 81−87.
(41) Ribierre, J. C.; Aoyama, T.; Muto, T.; Imase, Y.; Wada, T. *Org. Electron.* **2008**, *9*, 396−400.
(42) Xu, D.; Adachi, C. *Appl. Phys. Lett.* **2009**, *95*, 053304-1−053304-3.
(43) Ribierre, J. C.; Aoyama, T.; Muto, T.; André, P. *Org. Electron.* **2011**, *12*, 1800−1805.
(44) Watanabe, S.; Aoyama, T.; Fukuchi, Y.; Sassa, T.; Yamashita, T.; Matsumoto, M.; Wada, T. *J. Photopolym. Sci. Technol.* **2009**, *22*, 571−574.
(45) Watanabe, S.; Fukuchi, Y.; Fukasawa, M.; Sassa, T.; Uchiyama, M.; Yamashita, T.; Matsumoto, M.; Aoyama, T. *Langmuir* **2012**, *28*, 10305−10309.
(46) Yamamoto, S.; Guo, J.; Ohkita, H.; Ito, S. *Adv. Funct. Mater.* **2008**, *18*, 2555−2562.
(47) Guldi, D. M.; Prato, M. *Acc. Chem. Res.* **2000**, *33*, 695−703.
(48) Kaneto, K.; Abe, T.; Takashima, W. *Solid State Commun.* **1995**, *96*, 259−264.
(49) Chiesa, M.; Bürgi, L.; Kim, J.; Shikler, R.; Friend, R. H.; Sirringhaus, H. *Nano Lett.* **2005**, *5*, 559−563.
(50) Palermo, V.; Otten, M. B. J.; Liscio, A.; Schwartz, E.; Witte, P. A. J.; Castriciano, M. A.; Wienk, M. M.; Nolde, F.; Luca, G.; Cornelissen, J. J. L. M.; Janssen, R. A. J.; Müllen, K.; Rowan, A. E.; Nolte, R. J. M.; Samori, P. *J. Am. Chem. Soc.* **2008**, *130*, 14605−14614.

(51) Maturova, K.; Kemerink, M.; Wienk, M. M.; Charrier, D. S. H.; Janssen, R. A. J. *Adv. Funct. Mater.* **2009**, *19*, 1379−1386.
(52) Veltri, A.; Caputo, R.; Umeton, C.; Sukhov, A. V. *Appl. Phys. Lett.* **2004**, *84*, 3492−3494.
(53) Crellin, R. A.; Ledwith, A. *Macromolecules* **1975**, *8*, 93−101.
(54) Ellinger, L. P. *Polymer* **1964**, *5*, 559−578.
(55) Dzwilewski, A.; Wagberg, T.; Edman, L. *J. Am. Chem. Soc.* **2009**, *131*, 4006−4011.
(56) Wang, J.; Larsen, C.; Wangberg, T.; Edman, L. *Adv. Funct. Mater.* **2011**, *21*, 3723−3728.
(57) Luria, J. L.; Hoepker, N.; Bruce, R.; Jacobs, A. R.; Groves, C.; Marohn, J. A. *ACS Nano* **2012**, *6*, 9392−9401.
(58) Efimov, A.; Cohen, S. R. *J. Vac. Sci. Technol., A* **2000**, *18*, 1051−1055.
(59) Palermo, V.; Palma, M.; Samorì, P. *Adv. Mater.* **2006**, *18*, 145−164.